Physics of Plasmas ARTICLE pubs.aip.org/aip/pop

Nonlinear periodic ion-acoustic waves in nonthermal plasmas

Cite as: Phys. Plasmas **31**, 032305 (2024); doi: 10.1063/5.0189917
Submitted: 1 December 2023 · Accepted: 19 February 2024 ·
Published Online: 7 March 2024

Frank Verheest[1,2,a] and Carel P. Olivier[3,b]

AFFILIATIONS

[1]Sterrenkundig Observatorium, Universiteit Gent, Krijgslaan 281, B-9000 Ghent, Belgium
[2]School of Chemistry and Physics, University of KwaZulu-Natal, Scottsville, Pietermaritzburg 3209, South Africa
[3]Pure and Applied Analytics, School of Mathematical and Statistical Sciences, North-West University, Mahikeng Campus, Mmabatho 2745, South Africa

[a]Author to whom correspondence should be addressed: frank.verheest@ugent.be
[b]Electronic mail: carel.olivier@nwu.ac.za

ABSTRACT

A Sagdeev pseudopotential analysis is developed for the propagation of nonlinear periodic ion-acoustic waves in a plasma comprising cold fluid ions and various models of nonthermal electron descriptions. In plasma nonlinear wave studies, whether addressing solitary or periodic modes, the more common nonthermal distributions are the Cairns, kappa, and Tsallis models. A mathematically and physically consistent description incorporates three evident properties: there is conservation per cycle of ion and electron densities in addition to ion flux, the solutions reduce for very small amplitudes to linear waves, and the nonlinear periodic structures are generated by a perturbation of the undisturbed equilibrium. After establishing the corresponding general analytical methodology, a numerical analysis is given, with illustrative graphs, for the nonthermal Cairns, superthermal kappa, and nonextensive Tsallis distributions.

I. INTRODUCTION

Theoretical nonlinear plasma wave studies over the last half century encompass a vast literature on electrostatic solitary waves (solitons) in various plasma compositions. For solitons, single humps or dips, the area under the solitary curve representing the electrostatic potential in a co-moving frame is finite, regardless of the analytical method used, as far away from the nonlinear structure, the medium is as good as undisturbed. This means that solitons can be generated by relatively small perturbations from the undisturbed state, as is often observed in water or cloud waves in nature. This is briefly discussed later, after the following paragraph.

Nonlinear periodic structures have not received the same attention. These consist, of an infinite succession of humps and dips and to describe them one has to reason carefully. If there was an excess or loss of species' charge or mass densities over one cycle, that would then amount over an infinite number of cycles to an infinite excess or loss. Yet, this is not often worried about, giving the impression that a kind of solitary wave reasoning has been carried over, unwittingly but unjustified. While mathematicians could happily live with that and view it as a perfectly possible and correct description, for physicists, this is an untenable situation, where would the infinite mass excess density come from, or the infinite mass loss go to? What about the energy implications of this?

Such arguments point to an important distinction between perturbations of the undisturbed equilibrium, whether looking for solitary or for periodic nonlinear waves. As the soliton profile has a finite area under the curve, the energy and related quantities are finite, and the perturbation necessary to excite the wave can be contained to a small area of the spatial domain. For the periodic solitary waves, the picture and the conservation of densities, per cycle and overall, require a global perturbation, even though the relevant changes in maximum and minimum amplitudes might be small.

If one looks at the various treatments of nonlinear periodic structures in acoustic wave studies, one reaches the surprising conclusion that nobody seemed to have worried about the excess or loss of densities, until very recently the problem was realized and treated in three different papers.[1–3] These three papers contain references to the many papers where the analysis is not consistent from a physics point of view. As detailed comments were given earlier, the deficient papers will not be cited again here.

In the three recent papers,[1–3] the same cold ion model was used. The relative popularity of the cold ion model, not only in our earlier papers but also in the vast soliton literature, is that this leads to a simple but clear analytical description, yet producing interesting conclusions. The complications due to ion thermal effects do not, in general, matter qualitatively in a decisive way. It is the ion inertia, which is crucial to sustain ion-acoustic waves, linear or nonlinear. We feel, thus, justified to continue with the cold ion model, yielding the inertia.

As to the hot electron distributions that provide the pressure, the other prerequisite to sustain the waves, the three recent papers mentioned opted to use a Maxwellian model but treated the problem by various methods: reductive perturbation theory (RPT)[1] and two Sagdeev pseudopotential analyses (SPA). One of the latter[2] uses the Lambert W function[4] to obtain an analytical solution, while the other[3] follows a more conventional Sagdeev analysis[5] that allows the inclusion of other conservation laws than just the species' mass or charge densities and the possibility of extending the hot electron description.

Once one turns to hot electron models that are not Maxwellian, the Lambert W method does not work any longer, and, thus, the Sagdeev pseudopotential method used here will follow, in broad lines, the analysis of the preceding paper,[3] with appropriate generalizations and comments. The models all rely on the fact that for hot electrons, with their small mass, the nonthermal effects far outweigh the electron inertia, which is, thus, neglected.

Among the nonthermal distributions frequently encountered in the literature, three stand out: the Cairns nonthermal distribution,[6,7] the kappa superthermal distribution,[8–12] and the more recent (at least in plasma wave studies) Tsallis distribution.[13–17] It is those three that we will study in detail to see how they modify the conclusions compared to models with Maxwellian electrons.

One encounters in the literature also several combinations of the above-mentioned nonthermal ones, such as the Cairns–Tsallis distribution,[18,19] but we feel that these are quite artificial, without proper physical motivation. Moreover, in these combined distributions, the range of admissible Tsallis parameters q is more restricted, leading to a more complicated mathematical analysis with no gain in physical understanding.

In addition, periodic electric field signals have been reported in many regions of Earth's magnetosphere (see, for example, Rufai,[20] Singh *et al.*,[21] and references therein).

The paper is organized as follows: After this Introduction, Sec. II gives the analytical exposition of the problem, and Sec. III deals with the numerical results and graphical visualizations. Section IV contains our concluding remarks.

II. BASIC SAGDEEV ANALYSIS

As explained already, we consider the model of a plasma consisting of cold, singly charged ions, and nonthermal electrons and start with the normalized ion continuity and momentum equations,

$$\frac{\partial n_i}{\partial t} + \frac{\partial}{\partial x}(n_i u_i) = 0, \tag{1}$$

$$\frac{\partial u_i}{\partial t} + u_i \frac{\partial u_i}{\partial x} + \frac{\partial \varphi}{\partial x} = 0, \tag{2}$$

coupled by Poisson's equation

$$\frac{\partial^2 \varphi}{\partial x^2} + n_i - n_e = 0. \tag{3}$$

The electron models for n_e will be explicited below.

The notations have the usual meaning, and the normalization is the standard one for ion-acoustic waves.[3] As an important technical remark, when velocities are normalized by an ion-acoustic speed, written for simplicity as $(T_e/m_i)^{1/2}$, we have to remember that the measure for the kinetic temperature T_e (including the Boltzmann constant κ_B) used here is only a true electron kinetic temperature for Maxwellian electrons. For other descriptions, the definition of the (kinetic) temperature will vary with the electron thermal description, and, therefore, correction factors will be needed, depending on the proper modeling, to be discussed in Sec. III. With these normalizations, the undisturbed equilibrium plasma conditions are $n_i = n_e = 1$, $u_i = 0$, and $\varphi = 0$.

For coherence and, above all, readability of the present paper, we follow closely some of the analysis given in an earlier paper,[3] generalizing where necessary. The profiles φ of the periodic structures, as functions of a co-moving coordinate $\xi = x - vt$, alternate between a negative minimum φ_{min} and a positive maximum φ_{max} around $\varphi = 0$. Transforming the basic equations (1)–(3) to ordinary differential equations (ODEs) in ξ yields

$$-v\frac{dn_i}{d\xi} + \frac{d}{d\xi}(n_i u_i) = 0, \tag{4}$$

$$-v\frac{du_i}{d\xi} + u_i\frac{du_i}{d\xi} + \frac{d\varphi}{d\xi} = 0, \tag{5}$$

$$\frac{d^2\varphi}{d\xi^2} + n_i - n_e = 0. \tag{6}$$

To present the conservation laws that the solutions have to obey, we start by integrating (6) over one wavelength L (to be defined below) of the periodic structure. This yields

$$\int_0^L (n_i - n_e)d\xi = -\int_0^L \frac{d^2\varphi}{d\xi^2}d\xi = \left.\frac{d\varphi}{d\xi}\right|_{\xi=0} - \left.\frac{d\varphi}{d\xi}\right|_{\xi=L} = 0, \tag{7}$$

because of the periodicity of the φ profile after one wavelength. Hence, there is conservation of the *global* density over one period, written as

$$\int_0^L n_i d\xi = \int_0^L n_e d\xi. \tag{8}$$

As noted before,[3] this conservation law is not dependent on the specific (singly charged) ion and/or electron descriptions, and we will now exploit this to our advantage. The unperturbed equilibrium densities are $n_i = 1$ and $n_e = 1$ for all ξ and would give L when integrated over one wavelength L. Thus, we impose a conservation of electron number density through

$$\int_0^L (n_e - 1)d\xi = 0. \tag{9}$$

In view of (8), this will automatically ensure that the ion density is also conserved. Consequently, charge and mass density conservation per species follows, too.

Another conservation law is that of ion flux $n_i u_i$, given by

$$\int_0^L n_i u_i d\xi = 0, \tag{10}$$

as the ion flux is zero in the undisturbed equilibrium state.

Because $d\varphi/d\xi = 0$ at the minimum and maximum values of $\varphi = \varphi_{min}$ and $\varphi = \varphi_{max}$, there necessarily is an intermediate value where the tangent $d\varphi/d\xi$ reaches a positive maximum $\alpha = d\varphi/d\xi|_{\xi=0} > 0$. This inflection point has been taken as the origin of the ξ-axis, which can be done without loss of generality. Consequently, $d^2\varphi/d\xi^2|_{\xi=0} = 0$.

Furthermore, we denote the function values at the inflection point as $n_i(0) = n_e(0) = \gamma$, $u_i(0) = u_0$, and $\varphi(0) = 0$, to be further elucidated as follows. It is important to stress again, as in earlier treatments,[1–3] that such perturbations cannot start at the equilibrium conditions themselves, lest one runs into the soliton boundary conditions.

Integrating (4) and (5) with the initial values given earlier suggests[3] that the mathematics can be written in terms of the compact variable $w = v - u_0$. Eliminating the terms containing u_i, thus, yields the ion density,

$$n_i = \frac{\gamma}{\sqrt{1 - \dfrac{2\varphi}{w^2}}}. \tag{11}$$

We are now in a position to clarify (10). The physical picture for flux conservation requires u_i in the frame where the wave velocity is v, denoted as $u_{i(v)}$. However, the mathematical evaluation in Sec. III will be based on the w velocity; consequently, the numerics will give a different ion velocity, denoted as $u_{i(w)}$. Both ion velocity representations are related by $u_{i(w)} = u_{i(v)} - u_0$. Multiplying this by n_i and integrating that over one wavelength gives

$$\int_0^L n_i u_{i(w)} d\xi = \int_0^L n_i u_{i(v)} d\xi - u_0 \int_0^L n_i d\xi. \tag{12}$$

Conservation of flux requires $\int_0^L n_i u_{i(v)} d\xi = 0$, and since $\int_0^L n_i d\xi = L$, we determine simply that

$$u_0 = -\frac{1}{L}\int_0^L n_i u_{i(w)} d\xi, \tag{13}$$

yielding a unique value for u_0.

Together, we use conservation of density (9) and of ion flux (10) to obtain unique values for γ and u_0.

In order to have a generic description, we leave the details of the various nonthermal electron models for later and refer *in abstracto* to $n_e(\varphi)$, with $n_e(0) = \gamma$. At this stage, we mention a fundamental change in the way the electron density is obtained, compared to what happened in our earlier Sagdeev paper.[3] There, the basic assumption was that the electrons were isothermal ($n_e \propto p_e$), and their density was determined from the balance between the pressure and the electrostatic potential gradients in the momentum equation for massless electrons. That involved an integration over ξ and could, thus, introduce a nonzero constant φ_0, leading to the notation $\psi = \varphi - \varphi_0$, a procedure which would then to have a counterpart in the determination of n_i, as in our earlier Sagdeev paper.[3]

For the nonthermal electron distributions, the picture is different. These are defined first at the microscopic level in terms of electron velocity distributions and, in order to obtain a fluid description, are integrated over the phase space velocities, involving φ and yielding directly $n_e(\varphi)$. This means that there are no integration constants on φ in n_e, and for consistency, there cannot be one for n_i. Indeed, a $\varphi_0 \neq 0$ for n_i would introduce in (8) an arbitrary parameter on one side, not present on the other side, which is not consistent. For Maxwellian electrons and $\varphi_0 \neq 0$, one could invoke a conservation of φ over one wavelength to obtain a unique result, even though there was no physical argument requiring such a conservation but yielding a specific value φ_0. Here, that conservation law is not factored into the analysis.

Substitution of (11) into (6), multiplying the result by $d\varphi/d\xi$ and integrating with respect to ξ yields the Sagdeev energy-type conservation law,

$$\frac{1}{2}\left(\frac{d\varphi}{d\xi}\right)^2 + S(\varphi) = 0, \tag{14}$$

with the Sagdeev pseudopotential

$$S(\varphi) = \gamma w^2\left(1 - \sqrt{1 - \frac{2\varphi}{w^2}}\right) + \mathcal{N}_e(\varphi) - \frac{1}{2}\alpha^2, \tag{15}$$

where integration constants are obtained from the conditions at the inflection point $\xi = 0$. Here

$$\mathcal{N}_e(\varphi) = -\int_0^{\varphi} n_e(\chi)d\chi \tag{16}$$

with χ a dummy integration variable.

On the positive side, there is a limit for $\varphi \to \varphi_{lim} = w^2/2$, beyond which the ion density ceases to be real. Periodic waves oscillate between a negative and a positive extremum, which correspond to a negative and a positive root for $S(\varphi)$, with $S(\varphi) < 0$ in between. For a positive root, in view of the limitations imposed by the reality of the ion density, we need that

$$S(\varphi_{lim}) = \gamma w^2 + \mathcal{N}_e\left(\frac{w^2}{2}\right) - \frac{1}{2}\alpha^2 > 0. \tag{17}$$

$S(\varphi_{lim}) = 0$ can be solved for α as function of w,

$$\alpha^2 = 2\gamma w^2 + 2\mathcal{N}_e\left(\frac{w^2}{2}\right), \tag{18}$$

which yields minimum curves starting from $w = 0$ and $\alpha = 0$, where w increases with α, for values of γ and the nonthermality parameters. This will become explicit whenever we deal with a particular nonthermal model and obtain the expression for $\mathcal{N}_e(\varphi)$.

As in the earlier paper, on the negative side $S(\varphi) \to -\infty$ for $\varphi \to -\infty$, provided that $|\mathcal{N}_e(\varphi)|$ remains finite and bounded for negative φ. As will be shown, this condition is easily fulfilled for the models discussed later. Negative roots of $S(\varphi)$ come in pairs, and when the two negative roots nearest to $\varphi = 0$ coalesce, the limit on negative φ is reached. The conditions for that are

$$\begin{aligned} S(\varphi_{dl}) &= \gamma w^2\left(1 - \sqrt{1 - \frac{2\varphi_{dl}}{w^2}}\right) + \mathcal{N}_e(\varphi_{dl}) - \frac{1}{2}\alpha^2 = 0, \\ S'(\varphi_{dl}) &= \frac{\gamma}{\sqrt{1 - \dfrac{2\varphi_{dl}}{w^2}}} - n_e(\varphi_{dl}) = 0. \end{aligned} \tag{19}$$

A prime on $S(\varphi)$ denotes a derivative with respect to φ. First, $S'(\varphi_{dl}) = 0$ is solved for w^2 as function of φ_{dl}, giving

$$w^2 = \frac{2\varphi_{dl} n_e^2(\varphi_{dl})}{n_e^2(\varphi_{dl}) - \gamma^2}. \tag{20}$$

When this is substituted in $S(\varphi_{dl}) = 0$, the latter can be solved for α^2, yielding

$$\alpha^2 = 4\gamma \frac{\varphi_{dl} n_e(\varphi_{dl})}{n_e(\varphi_{dl}) + \gamma} + 2\mathcal{N}_e(\varphi_{dl}). \tag{21}$$

Contrary to the positive limit in (18), which is strictly tied to the reality of the ion density, the double layer limit might be considered a "soft" limit because α and w are implicit in φ_{dl}, which is treated in (20) and (21) as if it were a kind of dummy variable. Nevertheless, as in our earlier paper,[3] this double layer limit yields fairly indicative estimates.

Together, (20) and (21) give the maximal w as a function of α, to be shown by curves starting from some positive w at $\alpha = 0$, on which w decreases with increasing α. We now delimit a curved triangular region by the $\alpha = 0$ ordinate axis and the upper and lower curves giving w as function of α, larger than the lower and smaller than the upper curve. The maximum α is obtained where both limiting curves cross.

If the lower and the upper curves were not to cross (note that they cross for all models which have been numerically checked), we have to limit them to $\alpha < 1$; otherwise, the electrostatic potential profiles become double valued for given ξ. With this proviso, there always an existence domain in $\{\alpha, w\}$ space where periodic nonlinear waves that conserve the species' densities can exist. We stress that this conclusion holds for all (reasonable) electron distribution models, where n_e can be expressed as a function of φ, transcending the specific nonthermal distributions discussed later.

In our previous paper with Maxwellian electrons,[3] the numerical analysis has been checked for enough combinations of $\{\alpha, w\}$ inside the triangular region to justify that conclusion. This allows us to reduce the number of particular examples to be worked out here because in the nonthermal electron distributions, a new, nonthermality parameter has to be accommodated, in addition to α and w. Consequently, a too detailed parametric analysis would lead to a plethora of similarly looking figures and graphs, which are fairly easy to generate but give no additional insight and overload the graphical presentation. We, thus, restrict ourselves to selected α and w values near the three points of the curvilinear existence triangle, on the inside, and pick some representative values for the nonthermality parameters.

The three most commonly encountered nonthermal distributions in the plasma literature for $n_e(\varphi)$ yield, successively, the Cairns distribution,

$$n_C(\varphi) = \gamma(1 - \beta\varphi + \beta\varphi^2)\exp[\varphi], \tag{22}$$

the kappa distribution

$$n_\kappa(\varphi) = \gamma\left(1 - \frac{\varphi}{\kappa - 3/2}\right)^{-\kappa+1/2}, \tag{23}$$

and the more recent Tsallis distribution

$$n_T(\varphi) = \gamma[1 + (q-1)\varphi]^{(q+1)/(2q-2)}. \tag{24}$$

We, thus, start from the electron distributions as they are commonly encountered in the relevant literature.

For physical reasons, the nonthermal parameters have to obey restrictions: $0 \leqslant \beta < 4/7 \simeq 0.571$ (Cairns), $3/2 < \kappa < +\infty$ (kappa), or $1/3 < q < 1$ (Tsallis). These stem from the necessity to obtain convergent energy integrals at the macroscopic fluid level, when integrating over the phase space distributions, such that the concept of a temperature makes sense. These restrictions have been obeyed in the normalization and might have disappeared from sight but remain essential! The Maxwellian limit is obtained for $\beta = 0$, $\kappa \to +\infty$, and $q \to 1$, and for all three distributions, Poisson's equation yields $n_e(0) = \gamma$.

All this will be discussed in more detail in Sec. III.

III. DISCUSSION OF NUMERICAL RESULTS AND SOLUTION GRAPHS

In what follows, we will first establish the existence regions for the different parameters, typical for the type of nonthermal distributions, for chosen combinations α and w.

As mentioned already, the existence range in $\{\alpha, w\}$ space is a curvilinear triangle, with sides given by the $\alpha = 0$ axis, a lower limiting curve translating the reality of the ion density, and an upper limiting curve coming from the negative double layer limit in the Sagdeev pseudopotential. These curves vary with γ, and as we will find that the γ values needed to conserve the electron (or ion) density vary between 1 and 1.5, the curves in Figs. 1, 3, and 5 have been drawn for $\gamma = 1$ and various nonthermality parameters.

In Figs. 1–6 in this paper, we have used the same color coding. Blue is for high nonthermality parameters, chosen here as follows: $\beta = 0.5$, where the limit is $\beta < 4/7$; $\kappa = 2$, where the limit is $\kappa > 3/2$; and $q = 0.4$, where the limit is $q > 1/3$. Green is for the Maxwellian limit, reached for $\beta = 0$, $\kappa \to \infty$, and $q \to 1$. Red is for typical average nonthermality parameters between the highly nonthermal and Maxwellian values, in order to show the intermediate trends, and relying on the continuity of the various functions involved.

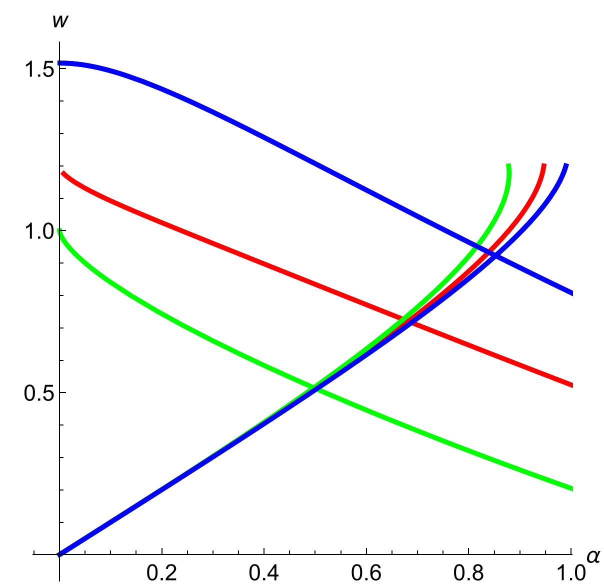

FIG. 1. Limiting curves for Cairns nonthermal parameters $\beta = 0.5$ (blue), 0.3 (red), and 0 (green) for $\gamma = 1$.

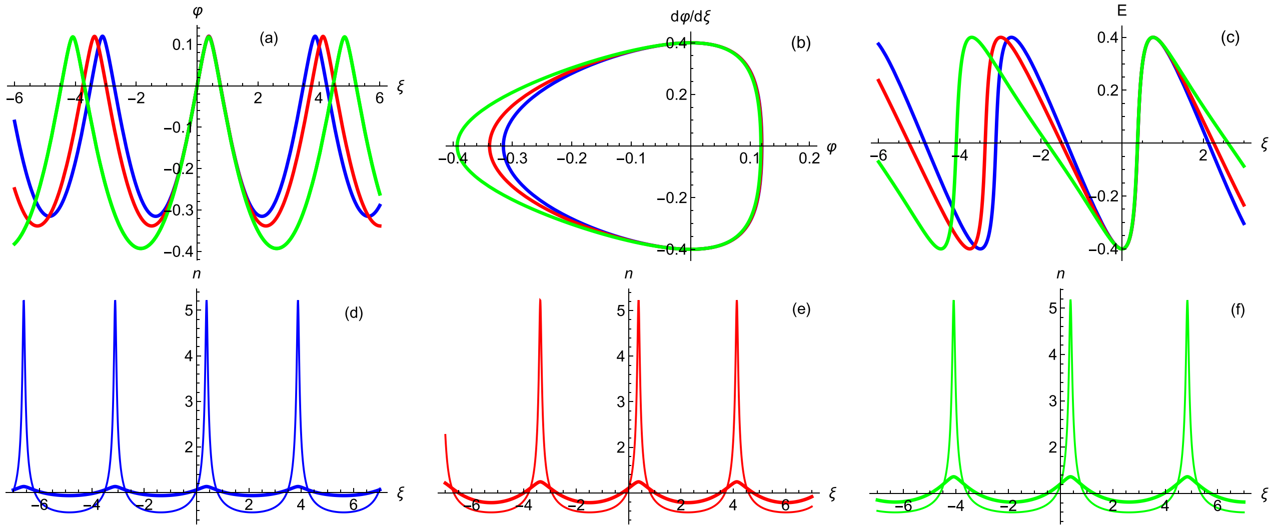

FIG. 2. Top row: (a) periodic profiles, (b) hodographs, and (c) electric fields, for Cairns electron distributions with typical nonthermality parameters $\beta = 0.5$ (blue), $\beta = 0.3$ (red), and $\beta = 0$ (green). Bottom row: electron (thick) and ion (thin) density profiles for (d) $\beta = 0.5$ (blue), (e) $\beta = 0.3$ (red), and (f) $\beta = 0$ (green). Other parameters are given in Table I.

Because the limiting curves change with variations in the nonthermality parameters, the rightmost corner of the triangle will limit α for an average w, whereas for small α, the topmost curve limits w. The lowermost corner near $\alpha = 0$ and $w = 0$ gives very weak periodic waves, which vary only little from one nonthermal model to the next or to a Maxwellian, and, thus, is not a physically exciting case.

We have also checked on all the worked-out examples that the global density conservation in (7) and (8) is correctly obeyed.

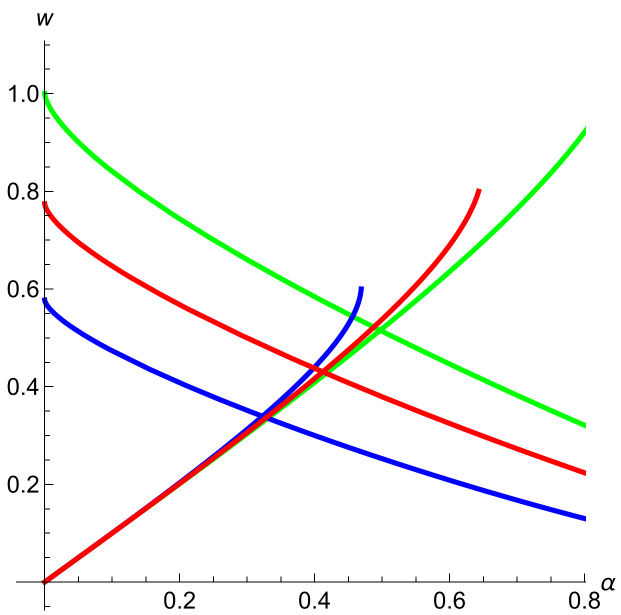

FIG. 3. Limiting curves for κ superthermal parameters $\kappa = 2$ (blue), 3 (red), and ∞ (green), for $\gamma = 1$.

A. Cairns nonthermal distributions

The Cairns distribution,[6] commonly used in theoretical space plasma studies, models a Maxwellian with an enhanced nonthermal tail, which may be characterized at the macroscopic level by a parameter β.[7] Cairns *et al.* introduced this velocity distribution function[6] to model the excess of superthermal particles often observed in space plasmas, as an *ad hoc* vehicle to explore their effects on nonlinear waves in space. The upper limiting condition $\beta < 4/7$ originates from wings appearing in the underlying phase space distribution for $\beta > 4/7$; in other words, the phase space distribution becomes triple-humped. Such a ring component might eventually become beam unstable.[7]

For the Cairns model, we set $n_e(\chi) = n_C(\chi)$, given by (22). Using this form of the electron density, we can evaluate the integral (16) to obtain

$$\mathcal{N}_C(\varphi) = \gamma\Big\{1 + 3\beta - (1 + 3\beta - 3\beta\varphi + \beta\varphi^2)\exp[\varphi]\Big\}, \tag{25}$$

such that $\mathcal{N}_C(0) = 0$ and $\lim_{\varphi\to-\infty}\mathcal{N}_C(\varphi) = \gamma(1 + 3\beta)$. The acoustic speed correction factor is

$$\sqrt{\frac{1}{1-\beta}}, \tag{26}$$

because when multiplied by $(T_e/m_i)^{1/2}$, it yields the true ion-acoustic speed under the Cairns distribution assumption. Recall that T_e has been used as a common normalizing temperature value but is only a correct thermal temperature in the Maxwellian limit. Thus, for other distributions, a correcting factor is needed, which will impinge on the maximum velocities. This correction factor is larger than 1 for the Cairns nonthermal model with $\beta < 4/7$, which has to be kept in mind when discussing supersonic or subsonic wave velocities, and goes to 1 when $\beta \to 0$.

The restrictive curves and the resulting existence triangle are shown in Fig. 1, for representative parameter values of β, all for $\gamma = 1$.

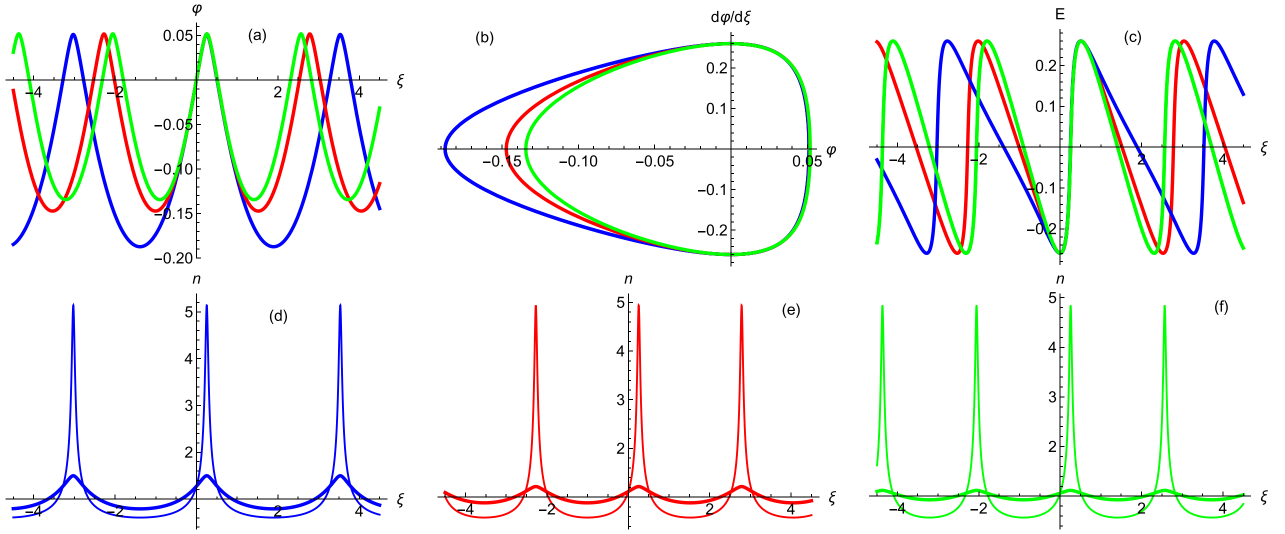

FIG. 4. Top row: (a) periodic profiles, (b) hodographs, and (c) electric fields, for kappa electron distributions with typical nonthermality parameter $\kappa = 2$ (blue), $\kappa = 3$ (red), and $\kappa \to \infty$ (green). Bottom row: electron (thick) and ion (thin) density profiles, in (d) $\kappa = 2$ (blue), (e) $\kappa = 3$ (red), and (f) $\kappa \to \infty$ (green). Further parameters are given in Table II.

It is seen that the existence domain covers larger areas as the nonthermality parameter β increases. Thus, the maximum α also increases, together with w on the crossing point of the two curves.

Interestingly, as $\alpha \to 0$, i.e., the small amplitude/linear regime, the upper limit seems to approach the true acoustic speed, which has been augmented by the correction factor due to the nonthermal Cairns distribution. As the lower limit approaches zero, this covers exactly the existence region of linear waves! (The same seems true for the other electron distributions). All in all, the waves remain subsonic.

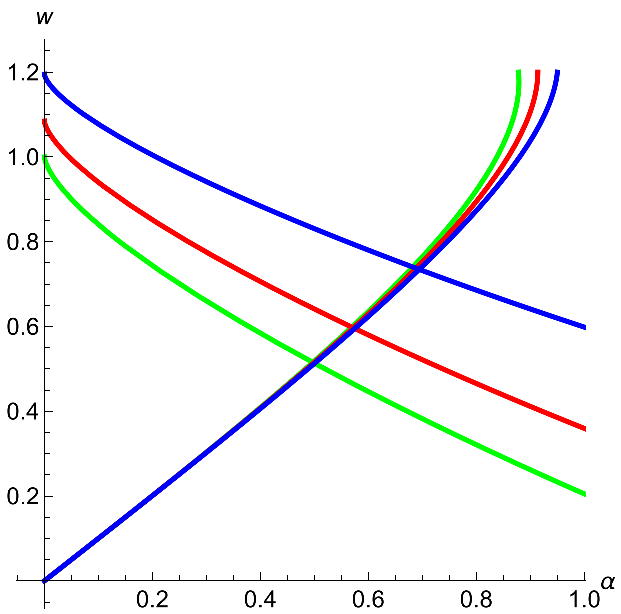

FIG. 5. Limiting curves for Tsallis nonextensive parameters $q = 0.4$ (blue), 0.7 (red), and 1 (green), for $\gamma = 1$.

With this in mind, we have computed in Table I for selected values of the nonthermality parameter β, maximum inflection α, and typical speed w. The resulting values of the ion density at the inflection point γ, the wavelength L, and a measure for the wave amplitude $\Phi = \varphi_{max} - \varphi_{min}$ are shown for each choice.

The numerical method we used starts by picking a pair of α, w values and numerically integrating Poisson's equation (6), using the various intermediate expressions. Equation (9) is then evaluated by trial-and-error until a unique γ gives a zero result. Interestingly, (8) is obeyed to a high degree of precision, even though the ion density (11) and the various electron densities (22)–(24) have quite different expressions. This result is, of course, completely predicted by the theory, thus indicating that the numerics match the theory.

The first three rows of Table I are for the more extreme parameters, specially for the largest α and corresponding w. To get a clearer view of the trends under changing β, we have chosen in the next three rows a common $\alpha = 0.4$ and $w = 0.5$, a range limited from below because of the inclusion of the Maxwellian. Here, it is clear that as the nonthermality increases, the three parameters γ, L, and Φ decrease. In the penultimate three rows $\alpha = 0.1$, w increases with the nonthermality, whereas γ decreases, but L and Φ increase. Finally, the bottom three rows are for the same small $\alpha = 0.1$ and $w = 0.2$, with different conclusions: γ, L, and Φ decrease as β increases. However, for such low values of α and w, the influence of nonthermality is hardly noticeable.

A similar methodology will be applied to Tables II and III, where the kappa-distributed electrons and Tsallis-distributed electrons are considered, respectively.

We have chosen $\alpha = 0.4$ and $w = 0.5$ to illustrate in Fig. 2 the influence of varying β on the profiles of large-amplitude periodic waves, hodographs, electric fields, and, most importantly, the electron and ion densities.

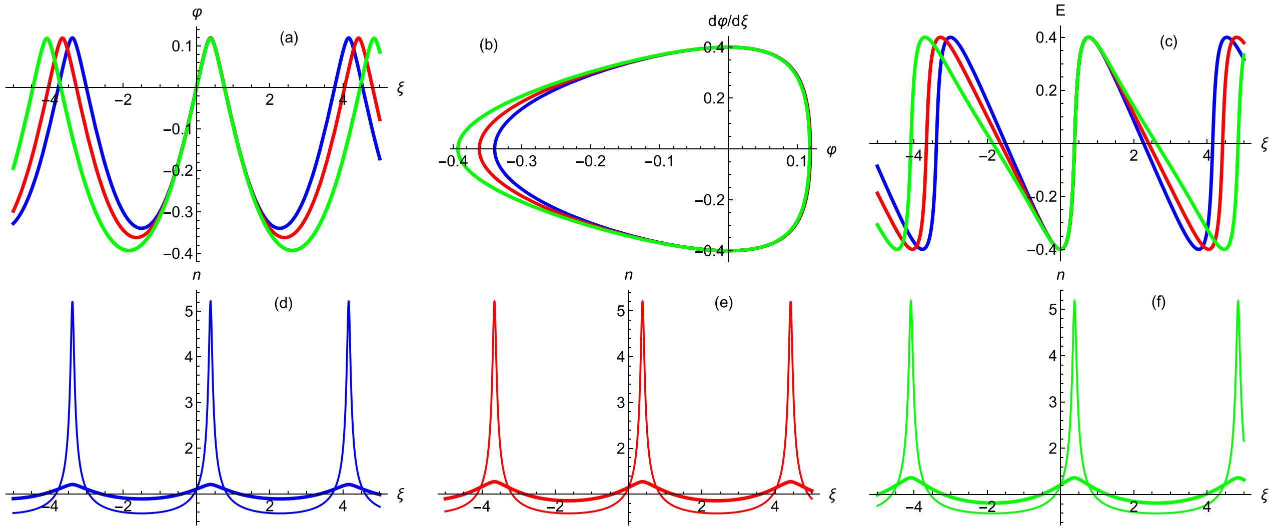

FIG. 6. Top row: (a) periodic profiles, (b) hodographs, and (c) electric fields, all for Tsallis electron distributions with typical nonextensivity parameter $q = 0.4$ (blue), $q = 0.7$ (red), and $q = 1$ (green). Bottom row: electron (thick) and ion (thin) density profiles, (d) $q = 0.4$ (blue), (e) $q = 0.7$ (red), and (f) $q = 1$ (green). Further parameters are given in Table III.

For the same combination $\{\alpha, w\}$, it is seen that increasing β results in decreasing γ, L, and Φ. The nonthermality helps to generate nonlinear periodic structures from a smaller perturbation.

B. Kappa superthermal distributions

Another way of modeling particle distributions with a high energy tail, which can deviate significantly from a Maxwellian, is a kappa or generalized Lorentzian distribution function[8–10] that appears to be more appropriate than a thermal Maxwellian distribution in a wide range of plasma situations. Both space and laboratory plasma environments may have such an excess superthermal electron population due to velocity space diffusion, leading to an inverse power-law distribution at a velocity much higher than the electron thermal speed. The kappa distribution has, thus, been widely adopted to model observed distributions.[11,22]

Because of this interest, Saini *et al.*[23] gave a thorough discussion of what replacing a Maxwellian by a kappa distribution for the electrons entails for ion-acoustic solitary modes in a two-component plasma. In the limit $\kappa \to \infty$, the kappa distribution reduces to a Maxwellian, much as the Cairns distribution does for $\beta = 0$.

Now working out (16) with (23) in the integrand yields

TABLE I. Typical α, w, β, γ, wavelength L, and global amplitude Φ of periodic nonlinear waves, for various Cairns distributions.

β	α	w	γ	L	Φ
0.5	0.86	0.90	1.309 144	8.904 74	2.136 82
0.3	0.68	0.70	1.394 999	7.621 56	1.390 73
0	0.46	0.50	1.288 323	4.801 54	0.607 65
0.5	0.4	0.5	1.059 037	3.492 65	0.435 11
0.3	0.4	0.5	1.102 851	3.754 46	0.457 96
0	0.4	0.5	1.211 279	4.464 72	0.511 12
0.5	0.1	1.20	1.002 460	14.063 60	0.449 35
0.3	0.1	1.00	1.031 233	12.05110	0.37532
0	0.1	0.80	1.053 868	9.485 74	0.285 87
0.5	0.1	0.20	1.003 779	1.272 95	0.040 46
0.3	0.1	0.20	1.005 432	1.279 88	0.040 65
0	0.1	0.20	1.008 020	1.290 62	0.040 94

TABLE II. Typical κ, α, w, γ, wavelength L, and global amplitude Φ of periodic nonlinear waves, for various kappa distributions.

κ	α	w	γ	L	Φ
2	0.32	0.33	1.422 926	3.734 57	0.312 51
3	0.40	0.42	1.370 173	4.463 93	0.474 96
∞	0.46	0.50	1.288 323	4.801 54	0.607 65
2	0.26	0.33	1.275 259	3.280 09	0.238 36
3	0.26	0.33	1.114 066	2.528 54	0.198 89
∞	0.26	0.33	1.061 498	2.311 73	0.186 21
2	0.05	0.45	1.024 852	4.633 99	0.073 42
3	0.05	0.65	1.025 875	7.977 47	0.123 78
∞	0.05	0.80	1.011 795	8.600 20	0.135 39
2	0.05	0.10	1.005 862	0.640 83	0.010 17
3	0.05	0.10	1.003 203	0.635 17	0.010 10
∞	0.05	0.10	1.001 906	0.632 40	0.010 06

TABLE III. Typical q, α, w, γ, wavelength L, and global amplitude Φ of periodic nonlinear waves, for various Tsallis distributions.

q	α	w	γ	L	Φ
0.4	0.68	0.71	1.439 196	8.244 71	1.466 64
0.7	0.50	0.60	1.307 439	6.133 08	0.836 14
1	0.46	0.50	1.288 323	4.801 54	0.607 65
0.4	0.4	0.5	1.105 532	3.763 96	0.458 92
0.7	0.4	0.5	1.148 507	4.041 05	0.480 83
1	0.4	0.5	1.211 279	4.464 72	0.511 12
0.4	0.05	1.05	1.013 623	14.251 60	0.223 89
0.7	0.05	0.91	1.012 906	10.832 60	0.170 26
1	0.05	0.80	1.011 795	8.600 20	0.135 39
0.4	0.05	0.1	1.001 324	0.631 16	0.010 04
0.7	0.05	0.1	1.001 614	0.631 78	0.010 05
1	0.05	0.1	1.001 906	0.632 40	0.010 06

$$\mathcal{N}_\kappa(\varphi) = \gamma\left[1 - \left(1 - \frac{\varphi}{\kappa - 3/2}\right)^{-\kappa+3/2}\right], \tag{27}$$

such that $\mathcal{N}_\kappa(0) = 0$ and $\lim_{\varphi\to-\infty}\mathcal{N}_\kappa(\varphi) = \gamma$. This distribution involves a true acoustic speed correction

$$\sqrt{\frac{2\kappa - 3}{2\kappa - 1}}. \tag{28}$$

Here, the correction is smaller than 1, so that the correction increases to 1 for the Maxwellian limit when $\kappa \to \infty$. This is contrary to what happens for Cairns or Tsallis distributions.

Figure 3 shows an inverse behavior, where the triangular existence domains increase as the superthermality decreases (κ increasing). Here, too, for $\alpha \to 0$, the linear wave regime is approached, as the true acoustic speed increases to 1.

In Table II, the same reasoning has been given as in Sec. III A, for different groups of $\{\alpha, w\}$ to show the different trends. For strictly the same combination $\{\alpha, w\}$ decreasing the superthermality results in lowering γ, L, Φ. This is precisely the opposite of what happens for the Cairns nonthermal electron distributions.

In Fig. 4, we have illustrated the different curves for the pair $\alpha = 0.26$ and $w = 0.33$.

C. Tsallis superextensive distributions

This brings us to the third of the commonly used nonthermal distributions with an enhanced non-Maxwellian "tail," the q-nonextensive distributions introduced by Tsallis.[13] Whereas the Cairns and kappa distributions are essentially empirical models, the Tsallis distribution, based on nonextensive statistical mechanics,[13] has the attraction that it may provide a rigorous theoretical foundation, although it appears that the approach is still somewhat controversial. However, we note that the Tsallis approach has also been linked to the kappa distribution.[12]

The family of Tsallis distributions, with a parameter q, has recently been much used in soliton theory, based on earlier linear wave studies,[14] but not always with the required care. The electron density $n_T(\varphi)$ in (24) has been obtained by integration of the Tsallis distribution in phase space over all velocities, the details of which are given elsewhere.[14,16,17] However, the restrictions on q that arise due to the convergence of some of the integrals need to be kept in mind because they are not visible when one inspects expressions like (24). The phase space distribution is unnormalizable for $q \leqslant -1$, just for the number density, but for $q \leqslant 1/3$, the energy integral diverges.[14,16,17]

This restriction is equivalent to the well-known limit $\kappa > 3/2$ that is always included by users of the kappa distribution.[10] This means that the nonextensive range has to be restricted to $1/3 < q < 1$, as for $q \to 1$, the Tsallis distribution reduces to a Maxwellian. Having a finite energy is necessary if one wants to introduce concepts like pressure and/or temperature in the fluid description of Tsallis species. Unfortunately, the restriction to $1/3 < q < 1$ is often not adhered to in numerical applications[17] and invalidates some of the conclusions in the literature. Between parentheses, in the range $q > 1$, the microscopic Tsallis distribution is only defined over a finite coordinate range around zero, which makes it unsuitable for the modeling of superthermal tails in space research and observations.

Thus, using (24) in (16) leads to

$$\mathcal{N}_T(\varphi) = \frac{2\gamma}{3q-1}\left\{1 - [1 + (q-1)\varphi]^{(3q-1)/(2q-2)}\right\} \tag{29}$$

with $\mathcal{N}_T(0) = 0$ and $\lim_{\varphi\to-\infty}\mathcal{N}_T(\phi) = 2\gamma/(3q-1)$. The true acoustic speed correction is now

$$\sqrt{\frac{2}{q+1}}, \tag{30}$$

which is greater than 1 for $q < 1$ but smaller than $\sqrt{3/2}$ for $q > 1/3$. This is clearly seen for the existence domains on the upper curves in Fig. 5. The linear waves are recovered for $\alpha \to 0$, with the true acoustic speed larger than 1.

As the nonextensive effects become weaker (for larger q) and tend ultimately to the Maxwellian value 1, Table III shows that for the

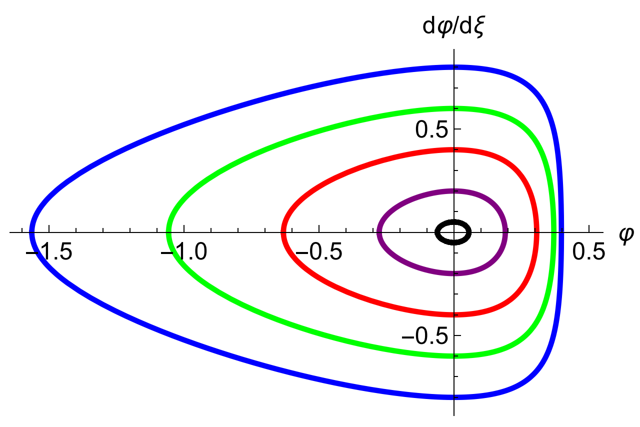

FIG. 7. Hodographs for strongly nonthermal Cairns electrons, with $\beta = 0.5$ and $w = 0.9$, for various α from large to small, namely, $\alpha = 0.8$ (blue), $\alpha = 0.6$ (green), $\alpha = 0.4$ (red), $\alpha = 0.2$ (purple), and $\alpha = 0.05$ (black). For very small α, the hodograph closely resembles what linear waves would produce.

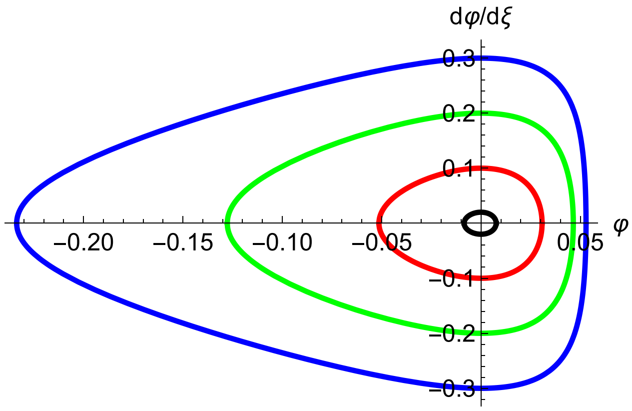

FIG. 8. Hodographs for strongly superthermal kappa electrons, with $\kappa = 2$ and $w = 0.33$, for various α from large to small, namely, $\alpha = 0.3$ (blue), $\alpha = 0.2$ (green), $\alpha = 0.1$ (red), and $\alpha = 0.02$ (black). For very small α, the hodograph closely resembles what linear waves would produce.

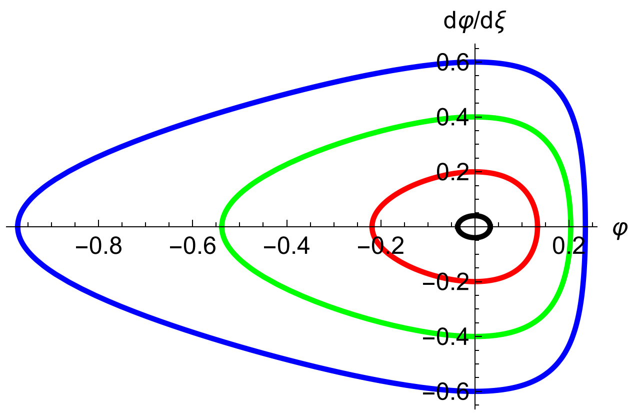

FIG. 9. Hodographs for strongly nonextensive Tsallis electrons, with $q = 0.4$ and $w = 0.33$, for various α from large to small, namely, $\alpha = 0.6$ (blue), $\alpha = 0.4$ (green), $\alpha = 0.2$ (red), and $\alpha = 0.04$ (black). For very small α, the hodograph closely resembles what linear waves would produce.

same $\{\alpha, w\}$ the parameters γ and properties L and Φ increase. This trend corresponds to what happens for the Cairns nonthermal electron distribution.

We have also illustrated in Fig. 6 the different curves for the pairs $\alpha = 0.4$ and $w = 0.5$.

D. Linear modes for small obliquity α

One of the desired characteristics of nonlinear periodic waves is that for small enough amplitudes, one rejoins the well-known linear waves; otherwise, there would exist in our understanding a conceptual gap between linear and nonlinear periodic waves. We now show in Figs. 7–9 on the hodographs for different sets of other parameters the approach to linear modes for very small values of α. This comes about in a natural way in our analysis—it has not been imposed or included *a priori*.

It is perfectly possible to go to even lower values of α than shown in Figs. 7–9, but then, the hodographs, resembling a clear ellipse when plotted on their own, would reduce to a mere blob on the scale of the larger ones in Figs. 7–9. These ellipses are associated with sinusoidal profiles of φ, in agreement with linear theory.

IV. CONCLUSIONS

One of the conclusions is that we now are firmly convinced that other electron distributions, if given in the form of $n_e(\varphi)$, will lead to analogous results about nonlinear periodic acoustic waves, and their treatment will be doable at the cost of added mathematical intricacy. The repetitivity of the various figures obtained here illustrates this very well.

The periodic nonlinear ion-acoustic waves in plasmas with nonthermal electrons show the same salient characteristics as for the Maxwellian electron model. These are (a) the conservation of species densities per cycle and (b) mimicking linear wave properties for very small obliquity, also at the strongest nonthermalities permitted by the respective descriptions. Characteristic (a) has, of course, been imposed on the analytical and, thus, also numerical discussion, as an evident physical requirement that has too often been neglected or ignored. On the other hand, characteristic (b) follows from the mathematical and numerical analysis at small amplitudes. This is nice because in this way, the limiting link between nonlinear and linear ("linearized" in a more accurate terminology) is obtained. In the various erroneous treatments, the small amplitude limits cannot be connected with the undisturbed conditions, leaving, thus, a conceptual gap between linear and nonlinear periodic waves, for which there is no immediate answer.

ACKNOWLEDGMENTS

This work was based on the research supported in part by the National Research Foundation of South Africa (Grant No. 145712).

AUTHOR DECLARATIONS

Conflict of Interest

The authors have no conflicts to disclose.

Author Contributions

Frank Verheest: Conceptualization (equal); Formal analysis (equal); Writing – original draft (lead); Writing – review & editing (equal). **Carel Petrus Olivier:** Conceptualization (equal); Formal analysis (equal); Writing – original draft (supporting); Writing – review & editing (equal).

DATA AVAILABILITY

Data sharing is not applicable to this article as no new data were created or analyzed in this study.

REFERENCES

[1] C. P. Olivier and F. Verheest, "A new reductive perturbation formalism for ion acoustic cnoidal waves," J. Plasma Phys. **88**, 905880601 (2022).
[2] A. E. Dubinov, "On one widely-spread inaccuracy and its elimination in the theories of nonlinear electrostatic waves in plasmas based on the Sagdeev's pseudopotential approach," Plasma Phys. Rep. **49**, 362–369 (2023).

[3]F. Verheest and C. P. Olivier, "Sagdeev pseudopotential analysis of nonlinear periodic ion-acoustic plasma waves," Phys. Plasmas **30**, 082306 (2023).
[4]R. M. Corless, G. H. Gonnet, D. E. G. Hare, D. J. Jeffrey, and D. E. Knuth, "On the Lambert *W* function," Adv. Comput. Math. **5**, 329–359 (1996).
[5]R. Z. Sagdeev, "Cooperative phenomena and shock waves in collisionless plasmas," in *Reviews of Plasma Physics*, edited by M. A. Leontovich (Consultants Bureau, New York, 1966), Vol. 4, pp. 23–91.
[6]R. A. Cairns, A. A. Mamun, R. Bingham, R. Boström, R. O. Dendy, C. M. C. Nairn, and P. K. Shukla, "Electrostatic solitary structures in non-thermal plasmas," Geophys. Res. Lett. **22**, 2709–2712, https://doi.org/10.1029/95GL02781 (1995).
[7]F. Verheest and S. R. Pillay, "Large amplitude dust-acoustic solitary waves and double layers in nonthermal plasmas," Phys. Plasmas **15**, 013703 (2008).
[8]V. M. Vasyliunas, "A survey of low-energy electrons in the evening sector of the magnetosphere with OGO 1 and OGO 3," J. Geophys. Res. **73**, 2839–2884, https://doi.org/10.1029/JA073i009p02839 (1968).
[9]D. Summers and R. M. Thorne, "The modified plasma dispersion function," Phys. Fluids B **3**, 1835–1847 (1991).
[10]M. A. Hellberg, R. L. Mace, T. K. Baluku, I. Kourakis, and N. S. Saini, "Comment on 'Mathematical and physical aspects of Kappa velocity distribution' [Phys. Plasmas **14**, 110702 (2007)]," Phys. Plasmas **16**, 094701 (2009).
[11]V. Pierrard and M. Lazar, "Kappa distributions: Theory and applications in space plasmas," Sol. Phys. **267**, 153–174 (2010).
[12]G. Livadiotis and D. J. McComas, "Understanding kappa distributions: A toolbox for space science and astrophysics," Space Sci. Rev. **175**, 183–214 (2013).
[13]C. Tsallis, "Possible generalization of Boltzmann-Gibbs statistics," J. Stat. Phys. **52**, 479–487 (1988).
[14]J. A. S. Lima, R. Silva, Jr., and J. Santos, "Plasma oscillations and nonextensive statistics," Phys. Rev. E **61**, 3260–3263 (2000).
[15]G. Livadiotis and D. J. McComas, "Beyond kappa distributions: Exploiting Tsallis statistical mechanics in space plasmas," J. Geophys. Res. **114**, A11105, https://doi.org/10.1029/2009JA014352 (2009).
[16]E. Saberian and A. Esfandyari-Kalejahi, "Langmuir oscillations in a nonextensive electron-positron plasma," Phys. Rev. E **87**, 053112 (2013).
[17]F. Verheest, "Ambiguities in the Tsallis description of non-thermal plasma species," J. Plasma Phys. **79**, 1031–1034 (2013).
[18]M. Tribeche, R. Amour, and P. K. Shukla, "Ion acoustic solitary waves in a plasma with nonthermal electrons featuring Tsallis distribution," Phys. Rev. E **85**, 037401 (2012).
[19]G. Williams, I. Kourakis, F. Verheest, and M. A. Hellberg, "Re-examining the Cairns-Tsallis model for ion acoustic solitons," Phys. Rev. E **88**, 023103 (2013).
[20]O. R. Rufai, "Periodic low-frequency electric field structures in a magnetized non-thermal auroral plasma," Heliyon **5**, e01976 (2019).
[21]S. V. Singh, R. Rubia, S. Devanandhan, and G. S. Lakhina, "Nonlinear electrostatic waves in the auroral plasma," Phys. Scr. **95**, 075602 (2020).
[22]M. Hapgood, C. Perry, J. Davies, and M. Denton, "The role of suprathermal particle measurements in cross scale studies of collisionless plasma processes," Planet. Space Sci. **59**, 618–629 (2011).
[23]N. S. Saini, I. Kourakis, and M. A. Hellberg, "Arbitrary amplitude ion-acoustic solitary excitations in the presence of excess superthermal electrons," Phys. Plasmas **16**, 062903 (2009).